Decay of ^{178}Tl

M. W. Rowe[1], J. C. Batchelder[2], T. N. Ginter[1], K. E. Gregorich[1], F. Q. Guo[3], F. P. Heßberger[4], V. Ninov[1], J. Powell[1], K. S. Toth[5], X. J. Xu[1] and Joseph Cerny[1,3]

[1]*Nuclear Science Division, Lawrence Berkeley National Laboratory, Berkeley, California 94720.*
[2]*UNIRIB, Oak Ridge Associated Universities, Oak Ridge, Tennessee 37831.*
[3]*Department of Chemistry, University of California, Berkeley, California 94720.*
[4]*Gesellschaft Für Schwerionenforschung mbH, Darmstadt, Federal Republic of Germany.*
[5]*Physics Division, Oak Ridge National Laboratory, Oak Ridge, Tennessee 37831.*

The new isotope ^{178}Tl was produced in a bombardment of ^{102}Pd by ^{78}Kr ions at 340 MeV. Reaction products were separated from the beam by the Berkeley Gas-Filled Separator and implanted into a silicon strip detector where the subsequent alpha decays were measured. Four distinct alpha transitions from ^{178}Tl were observed correlated to 6.54 MeV alpha decays from the previously known ^{174}Au daughter. In some cases, the ^{174}Au decay was followed by a 5.815 MeV alpha decay. This new transition is tentatively assigned to the decay of the ^{170}Ir ground state. The half-life of ^{178}Tl was measured to be 254^{+11}_{-9} ms. The alpha decay branch of ^{174}Au was determined to be 90(6)%.

PACS number(s): 23.60.+e, 27.70.+q, 21.10.Tg

I. INTRODUCTION

Investigations of isotopes far from stability provide important data for the testing of various nuclear models. The properties of nuclei near closed shells are of particular theoretical interest. On-line mass separators used in concert with position-sensitive charged-particle detectors have made the study of proton- and alpha-particle emitters near and beyond the proton drip-line possible, despite the very short half-lives and low production cross sections typical of such nuclides [1]. These measurements reveal both mass and structure information at the extreme limits of nuclear stability.

Both proton and alpha-particle emission have been observed in the case of the lightest known thallium isotope, ^{177}Tl [2]. The only published information on the decay of ^{178}Tl is in a paper by Carpenter, *et al.* [3], describing measurements of excited states in ^{176}Hg and ^{178}Hg. Therein, they state, "...three other alpha lines at 6.71, 6.79 and 6.87 MeV are correlated with A = 178. These three lines, are, in turn, all followed by alpha decay to [*sic*] the same daughter nucleus, ^{174}Au. They have been associated with the decay of the previously unknown isotope ^{178}Tl." We report here detailed results of a more recent measurement of ^{178}Tl and its decay properties, which agree with the earlier measurement [3]. New information about the decays of nuclei in its decay chains is also presented.

II. EXPERIMENTAL METHOD

Thallium-178 was produced in a 355 MeV (340 MeV mid-target) ^{78}Kr bombardment of a fixed 1.05 mg/cm^2 90.4%-enriched ^{102}Pd target at Lawrence Berkeley National Laboratory's 88-Inch Cyclotron. This produced ^{180}Pb compound nuclei at an excitation energy of 32.5 MeV. The beam was pulsed so that decay spectra could be measured more cleanly during the beam-off period (particularly on-line), though decays were also measured when the beam was on. The beam-on and beam-off periods each lasted for 2 ms; this timing was chosen somewhat arbitrarily. A pair of detectors mounted behind the target monitored the elastic scattering rate to determine beam intensity. The average beam current was 34 pnA for a total beam dose of 3.9 x 10^{16} ions obtained over 51.5 hours. The beam was separated from reaction products and deposited inside the Berkeley Gas-Filled Separator (BGS) [4], depicted in Fig. 1. Fusion-evaporation residues (EVR's) exited the separator and passed through two parallel plate avalanche counters (PPAC's) before stopping in the focal plane detector. Signals from the PPAC's permitted ions implanted in the focal plane detector to be differentiated from decays. Time-of-flight (TOF) measurements between the two PPAC's and the focal plane detector further allowed EVR's to be distinguished from other beam-related implantation events.

The focal plane detector consisted of a 120 mm (horizontal) by 60 mm (vertical) by 300 μm silicon strip detector with 16 strips oriented vertically. By measuring signals from both ends of each strip and comparing them to the sum, resistive charge division permitted the vertical location of events in each strip to be determined to within 0.7 mm full-width at half maximum (FWHM). The detector was calibrated using the energies of known alpha emitters produced in the bombardment. Alpha-decay peaks were observed with a typical resolution of ±35 keV FWHM. The average implantation depth of the EVR's was approximately 6 μm. Because half of all alpha particles were emitted into the focal plane detector, the full-energy detection efficiency for alpha decays was about 50%. Of the alpha particles emitted out of the detector, approximately 40% produced sufficient signals to be observed. Two additional silicon strip detectors, identical in size to the focal plane detector, placed perpendicular to the focal plane detector along its upper and lower edges, permitted the full energy of these escaping alpha particles to be detected 40% of the time. However, the energy resolution for these alpha particles measured in

this way was 200 keV FWHM. Another identical silicon strip detector was placed immediately behind the focal plane detector. This permitted light, high-energy ions that were not stopped in the focal plane detector to be identified and rejected. These ions resulted from collisions between the beam and the helium atoms in the BGS. Two 50% high-purity germanium detectors for detecting x-rays and gamma rays were also mounted near the focal plane.

Ions implanted into the focal plane detector were identified in software through observation of their decay chains, correlated in time and position. As new events were measured they were classified by type (i.e., EVR, alpha decay, escape) and stored in a circular buffer for each strip. Time stamps for each event were generated using (semi-redundant) 1 MHz, 1 kHz and 1 Hz clocks. When a decay was observed, a search was made for earlier events at the same detector location (±0.7 mm). The search was terminated when either a correlated event was found or after a specific time period had elapsed. Depending on the energy of the decay, this period ranged from 0.5 to 20 s. If a correlation was found, the location of the daughter in the buffer was stored with the parent. Once the circular buffer had been filled, the oldest event in the buffer would have to be removed before the new event could be added. Prior to its removal, a check would be made to see if the old event had been correlated to a daughter, and if so, whether the daughter had been correlated to the grand-daughter. In this way, the entire decay chain of an EVR could be traced to its end. By looking within each chain for alpha-decay energies corresponding to specific parent/daughter pairs, decay chains of interest were identified and saved to file, and time and energy information was saved to spectra. The members of this old chain were then deleted and the new event was added to the buffer.

The average rates of implantations and alpha decays over the entire focal-plane detector were 50 Hz and 4 Hz, respectively. Taking into account that the distribution of events over the detector surface was not uniform, the mean times between implantations and between decays were 8.8 s and 110 s, respectively, at a specific location (±0.7 mm). Thus the probability of observing a random correlation was low for short-lived isotopes. However, observed half-lives, calculated from the distribution of decay times of isotopes in specific decay chains, were corrected for random alpha-particle and EVR rates. When using an algorithm where either a real or random correlation will halt the search for

additional correlations, the observed distribution of alpha decay times for a specific decay is:

$$\frac{dN}{dt} = \lambda e^{-(\lambda + R_{EVR} + R_\alpha)t} \tag{1}$$

where λ is the decay constant for the alpha decay of interest, and R_{EVR} and R_α are the rates of random EVR's and random alpha decays, respectively. This implies that the observed decay rate, as determined from a fit to the time distribution, is the sum of the true decay rate and the random decay rates. Furthermore, the correlation efficiency ε_{corr}, defined as the fraction of alpha decays successfully correlated to their parents, is given by the equation:

$$\varepsilon_{corr} = \left(\frac{\lambda}{\lambda + R_{EVR} + R_\alpha} \right) \left(1 - e^{-\lambda t_{search}} \right) \tag{2}$$

where t_{search} is the maximum correlation search time. Note that equation 2 assumes a detection efficiency of 100%.

Additionally, a Monte Carlo simulation of random correlations was incorporated into the analysis to aid in determining whether observed parent-daughter alpha decay pairs were likely due to real or random correlations. Following the search for correlations for each alpha decay observed, a random correlation probability was calculated based on the duration of the search, the number of alpha decays observed during the preceding minute, and the fraction of events at the particular detector position relative to the total detector surface (the position distribution of events). A random number between zero and one then determined whether a "random" correlation was generated. If so, a second random number generated a simulated "parent" alpha-decay energy from the distribution of parent energies observed during the bombardment. Using this and the energy of the observed alpha decay for the daughter, a random correlation spectrum, showing counts as a function of parent and daughter energies was incremented. For statistics, one thousand such trials were performed for each alpha decay.

III. RESULTS

The alpha decay spectrum measured during the beam-off period is shown in Fig. 2. Although the peaks in this spectrum often include several different, unresolved alpha-

decay lines, contributions from different isotopes were determined from known energies of parent/daughter decay pairs. Figure 3a shows the energy relationships between pairs of alpha decays occurring within 0.7 mm of the same location on the focal plane during a time interval of 20 s or less. The energy of the first, parent, decay, is plotted versus the energy of the second decay observed, which is usually the daughter decay, but may also be the decay of a subsequent member of the parent's decay chain. The latter situation may occur if the daughter undergoes beta decay, or if it emits an alpha particle out of the detector, so that the daughter decay is not observed. The intensity (z-axis) is displayed logarithmically. Random correlations have been subtracted based on the results of the Monte Carlo simulation, as described above. By combining the intensities of these peaks with knowledge of alpha branching ratios from the literature, the peaks in Fig. 2 were identified and used for a precise energy calibration. Peaks in Fig. 3a are labeled in Fig. 3b and identified in Table I.

The alpha decay spectra are dominated by decays of Hg and Pt isotopes, with weaker contributions from Au, Ir and Tl decays. Several peaks are assigned to isotopes with Z £ 75. These were produced from the bombardment of the target by a 296 MeV beam of $^{65}Cu^{15+}$ ions that was accelerated co-resonant with the ^{78}Kr beam. However, the residue nuclides that result from de-excitation of the ^{167}Re compound nucleus have relatively small alpha-decay branches and low alpha-decay energies (typically < 6 MeV), and thus did not significantly interfere with the analysis. Half-lives for a number of isotopes were remeasured with improved precision in the present work. The results are compared to literature values [5,6 and references cited therein] in Table II.

In Fig. 3, groups of closely spaced peaks are observed at parent energies ranging from 6.6 to 6.9 MeV and daughter energies of 6.54 MeV (peak 1) or 6.04 MeV (peak 2), which correspond respectively to the known decay energies of ^{174}Au (6.544 ±0.01 MeV [5]) and its beta-decay daughter, ^{174}Pt (6.038 ± 0.004 MeV [7].) To generate Fig. 4, software cuts were placed on the observed, random (neither shown) and real (i.e., Fig. 3) alpha-alpha correlation plots for specific daughter energies. In Figs. 4a and 4b, observed correlated events preceding 6.54 MeV and 6.04 MeV decays, respectively, are displayed, along with the simulated random-correlation distributions for these daughter energies (shaded). The number of random correlations associated with the 6.04 MeV decay is relatively large

because this is the most intense peak in the alpha-decay singles spectrum (see Fig. 2.) In Fig 4c, the real-correlation spectra, as calculated from the differences between the observed and simulated random-correlation spectra, are shown. The unshaded spectrum shows parent peaks associated with 6.54 MeV alpha particles, while the shaded spectrum shows the parents of 6.04 MeV alpha particles.

Four prominent peaks at energies of 6.616(15), 6.704(5), 6.785(5) and 6.859(5) MeV are observed correlated to 6.54 MeV alpha particles (unshaded spectrum in Fig. 4c.) These transitions are sometimes observed in coincidence with gold x-rays [8]. There are two intense peaks associated with the 6.038 MeV daughters, at 6.430 MeV and 6.280 MeV (shaded spectrum in Fig. 4c.) The former is from ^{178}Hg decays correlated with ^{174}Pt [9], while the latter results from ^{179}Hg decays correlated with the 6.038 MeV alpha transition of ^{175}Pt [9]. In this spectrum, there are also about 80 alpha decays between 6.5 MeV and 6.9 MeV, with an intensity distribution similar to those correlated to 6.54 MeV alpha particles. Because the decays between 6.5 and 6.9 MeV are followed by alpha decays corresponding to the decays of ^{174}Au and its beta-decay daughter, ^{174}Pt, they are assigned to the alpha decay of ^{178}Tl. The combined half-life of these transitions, corrected for random-correlation rates as per Equation 1, is 254^{+11}_{-9} ms; the half-lives associated with the individual peaks are consistent with this value. Table III lists the characteristics of these decays.

As discussed earlier, the correlation-search algorithm employed permitted entire decay chains to be examined, rather than just pairs of correlated decays. In Fig. 5, correlated alpha decays observed after ^{178}Tl decays are shown; the ^{178}Tl–^{174}Au and ^{178}Tl–(^{174}Au)–^{174}Pt decay chains are shown in parts a and b, respectively. In each case, calculated random-correlation intensities are also indicated. Figure 5a shows peaks at 6.538 MeV, 5.408 MeV and 5.815 MeV. The two former energies agree with the literature values for ^{174}Au [5] and ^{170}Os [7], respectively, while the latter energy is not associated with a member of the ^{178}Tl decay chain found in the literature. Figure 5b also shows a ^{170}Os peak at 5.407 MeV, as well as the 6.038 MeV peak associated with ^{174}Pt [7].

IV. DISCUSSION

Figure 6 depicts the decay scheme of ^{178}Tl deduced from these data. Thallium-178 decays to ^{174}Au by one of four alpha transitions of 6.616(15), 6.704(5), 6.785(5) or 6.859(5) MeV. The widths of the peaks observed suggest that there may be additional transitions between the 6.616 and 6.785 MeV peaks, that are not resolved. It is interesting to note that the next heavier odd-odd Tl isotope, ^{180}Tl, also decays by a number of closely spaced transitions [10]. Carpenter, *et al*. [3], observed three alpha transitions at 6.71, 6.79 and 6.87 MeV that they assigned to the decay of ^{178}Tl. These values are in excellent agreement with the present work. The agreement between the half-lives of the individual transitions, and the fact that only a single ^{174}Au transition is observed correlated with these decays tends to indicate that a single state in ^{178}Tl feeds four daughter states in ^{174}Au; there is no evidence of isomerism in either isotope. Unfortunately, no unambiguous gamma-ray transitions were observed correlated to these decays that would confirm this hypothesis. If one assumes that the 6.859 MeV transition (Q_α = 7.017 ±0.005 MeV) feeds the ground state of ^{174}Au (Δ = –14.05 ±0.15 MeV), this implies a ^{178}Tl mass excess of at least –4.61(15) MeV. This is in best agreement with the Aboussir, *et al*. (-4.60 MeV [11]), and Masson-Jänecke (-4.47 MeV [12]) mass predictions. This mass indicates that ^{178}Tl is unbound to proton emission by 0.83(19) MeV, as calculated from the known ^{177}Hg mass excess [13].

Although two ^{174}Au transitions, 6.544(10) MeV and 6.637(13) MeV, are found in the literature [5,14], only the former transition was observed correlated with ^{178}Tl decays in this work. If ^{174}Au decays by positron emission or electron capture rather than alpha emission, ^{178}Tl decays may be observed in coincidence with ^{174}Pt alpha decays. As shown in Fig. 4c, 1131 ^{178}Tl-^{174}Au correlated decays were observed, compared to 82 ^{178}Tl-^{174}Pt decays. Combining this with the 67(6)% alpha branch of ^{174}Pt measured by Page, *et al*. [5] and the correlation efficiencies for each decay, the alpha-decay branch of ^{174}Au is 90(6)%. The ^{102}Pd(^{78}Kr,pn)^{178}Tl cross section is at least 40 nb at 340 MeV, based on the total number of correlated decays observed, detection and correlation efficiencies, and a calculated BGS efficiency of 60%. This assumes that the (unknown) alpha-decay branch for ^{178}Tl is 100%, so the correct cross section is somewhat higher.

Several alpha decay energies are associated with ^{170}Ir, the ^{178}Tl grand-daughter, in the literature. The average of the older measurements, done using gas-transport methods, is 6.025(5) MeV [7,15,16]. In the first measurement of ^{174}Au decay by Schneider, *et al*. [14], no correlated ^{170}Ir decays were observed following the 6.540 MeV ^{174}Au transition. Page, *et al*. [5], observed two ^{170}Ir transitions at 6.003(10) MeV and 6.083(11) MeV; the latter was observed following 6.544(10) MeV ^{174}Au decays, while the former was not. In Fig. 3, peak O corresponds to 6.54 MeV alpha decays correlated to 6.08 MeV decays, in agreement with the observations of Page, *et al*. However, the 6.08 MeV decay was not conclusively observed as part of the ^{178}Tl decay chain in the present work. As shown in Fig. 5a, a few counts were observed in the region between 5.9 and 6.1 MeV, but they are not statistically significant. This is partially due to the large number of random correlations expected at these energies.

Figure 7 shows the energies of observed alpha decays among the lightest iridium isotopes as a function of mass number [17-19]. In several cases, two transitions are observed. In these isotopes, the low-energy transition has consistently been assigned to a low-spin ground state, whereas the high-energy decays have been assigned to high-spin isomers. The 5.815(10) MeV transition shown in Fig. 5a is indicated in this plot as a filled circle at A = 170. It is seen that this energy agrees very well with the systematics of the ground-state transitions seen among the other Ir isotopes. On this basis, and the fact that this decay is seen following the ^{178}Tl-^{174}Au decay chain, we assign this transition to the previously unobserved ground state of ^{170}Ir. This implies a ground-state mass excess of –23.48(15) MeV. A half-life of $0.87\ ^{+0.18}_{-0.12}$ s and an alpha decay branch of 5.2 ±1.7% were observed for this decay. It appears that the high-spin ^{170}Ir isomer is produced in high yield as a reaction product, whereas the alpha decay of ^{174}Au favors the presumably low-spin ground state due to the increased decay energy and perhaps a smaller change in angular momentum.

The 5.407(10) MeV and 5.408(15) MeV peaks observed in Figs. 5a and 5b, respectively, agree well with the literature energy for the decay of ^{170}Os, 5.407(4) MeV. Osmium-170 is produced as the beta-daughter of ^{170}Ir in the ^{178}Tl-^{174}Au decay chain depicted in Fig. 5a. It is also produced as the daughter of ^{174}Pt in the ^{178}Tl-^{174}Au-^{174}Pt decay chain shown in Fig. 5b. In this latter case, the number of ^{170}Os counts observed

agrees with expectations on the basis of the ^{170}Os alpha branching ratio of 8.6(6)% [5]. It should be noted that when this branching ratio is combined with the number of 5.815 MeV and 5.405 MeV events observed in Fig. 5a, the correlation efficiencies as described by Equation 2 and the detection efficiency, the decays of all of the ^{170}Ir atoms resulting from the observed ^{174}Au decays are accounted for.

The 6.54 MeV and 5.82 MeV decay pair assigned to the new ^{170}Ir transition is indicated as peak 3 in Fig. 3. Based upon the systematics of correlated Au and Ir decays in this mass region, as revealed by peaks 3 and O, R and Q, and S and T in Fig. 3, we tentatively assign peak 4 in this spectrum to the ^{171}Ir^{g}/^{175}Au decay pair (the ^{171}Ir^{m}/^{175}Au pair is indicated by peak P.) The 5.717(10) MeV transition is indicated in Fig. 7 as a filled circle at A = 171, where it agrees with the general trend for Ir ground-state decays[†]. No other pair of decays has been found in the literature to account for peak 4. Unfortunately, correlated decays preceding or following this pair, which would confirm this assignment, were not observed. This is explained by the low yield of ^{179}Tl produced and the small alpha-decay branches of the ^{171}Ir daughters. The half-life measured for this transition is $3.2^{+1.3}_{-0.7}$ s. The alpha decay energy of ^{171}Ir implies a ground-state mass of –26.59(14) MeV.

A comparison between the experimental masses of ^{178}Tl, ^{170}Ir and ^{171}Ir deduced from these results, and the predictions of various mass models and relations is shown in Table IV.

V. CONCLUSION

Thallium-178 was produced from the ^{102}Pd(^{78}Kr,pn)^{178}Tl reaction with a cross section of at least 40 nb at 340 MeV. We have measured four alpha-decay transitions, which are correlated to either ^{174}Au or ^{174}Pt alpha decays, that we assign to the decay of ^{178}Tl. The energies agree with another measurement mentioned briefly in the literature [3]. Based on the agreement between the combined half-life of 254^{+11}_{-9} ms, and the half-lives

[†] It is interesting to note that the spectrum shown in Fig. 5 of Ref. 15, which resulted from a 280 MeV ^{63}Cu bombardment of a ^{108,110,111}Cd target, has unassigned alpha transitions at 5.81 MeV and ~5.72 MeV(unlabelled). These energies are in excellent agreement with the 5.815 MeV and 5.717 MeV decays assigned to ^{170}Ir^{g} and ^{171}Ir^{g}, respectively, in the present work. In Ref. 15, assignments were inferred on the basis of excitation function measurements and cross bombardments.

observed for the individual transitions, we conclude that the decays feed four daughter states in ^{174}Au. Assuming that the highest energy transition feeds the ground state leads to a lower limit of –4.61(15) MeV for the ^{178}Tl mass excess. This value agrees well with some mass predictions in the literature. Based on the relative number of ^{178}Tl-^{174}Au and ^{178}Tl-^{174}Pt correlated decays, and the known ^{174}Pt branching ratio, we deduce a 90(6)% alpha branch for ^{174}Au. Among the decays observed in the ^{178}Tl decay chains is a 5.815(10) MeV transition that we assign to the ground state of ^{170}Ir, which implies a mass excess of –23.48(15) MeV.

ACKNOWLEDGMENTS

The authors wish to thank D. Strellis, N. K. Seward and P. A. Wilk for working shifts during the measurement. We thank the 88" Cyclotron operations staff for the excellent beam they provided, and the technical staff for their support in this experiment. We also thank B. Kindler and B. Lommel of G.S.I Darmstadt for fabricating the ^{102}Pd target. This work was supported by the U. S. Department of Energy, Division of Nuclear Physics under contracts DE-AC03-76SF00098 (Lawrence Berkeley National Laboratory), DE-AC05-76OR00033 (UNIRIB), and DE-AC05-96OR22464 (Oak Ridge National Laboratory, managed by Lockheed Martin Energy Research Corporation).

REFERENCES

1. P. J. Woods and C. N. Davids, Ann. Rev. Nucl. Part. Sci. **47**, 541 (1997).
2. G. L. Poli, *et al*., Phys. Rev. C **59**, R2979 (1999).
3. M. P. Carpenter, *et al*., Phys. Rev. Lett. **78**, 3650 (1997).
4. M. W. Rowe, *et al*., in "Proton-Emitting Nuclei First International Symposium," J. C. Batchelder, ed., pp. 95-104 (AIP Conference Proceedings 518, Melville, New York, 2000.)
5. R. D. Page, P. J. Woods, R. A. Cunningham, T. Davinson, N. J. Davis, A. N. James, K. Livingston, P. J. Sellin and A. C. Shotter, Phys. Rev. C **53**, 660 (1996).
6. P. M. Davidson, G. D. Dracoulis, T. Kibédi, A. P. Byrne, S. S. Anderssen, A. M. Baxter, B. Fabricius, G. J. Lane, A. E. Stuchbery, Nucl.Phys. A**657**, 219 (1999).

7. A. Rytz, At. Data Nucl. Data Tables **47**, 205 (1991).
8. R. B. Firestone, "Table of Isotopes, 8th ed.," V. S. Shirley, ed., vol. II, p. F-46 (John Wiley and Sons, New York, 1996.)
9. E. Hagberg, P. G. Hansen, P. Hornshøj, B. Jonson, S. Mattsson and P. Tidemand-Petersson, Nucl. Phys. **A318**, 29 (1979).
10. K. S. Toth, *et al*., Phys. Rev. C **58**, 1310 (1998).
11. Y. Aboussir, J. M. Pearson, A. K. Dutta and F. Tondeur, At. Data Nucl. Data Tables **61**, 127 (1995).
12. P. E. Haustein, ed., At. Data Nucl. Data Tables **39**, 186 (1988).
13. G. Audi and A. H. Wapstra, Nucl. Phys. **A595**, 409 (1995).
14. J. R. H. Schneider, S. Hofmann, F. P. Heßberger, G. Münzenberg, W. Reisdorf and P. Armbruster, Z. Phys. A **312**, 21 (1983).
15. C. Cabot, S. Della Negra, C. Deprun, H. Gauvin and Y. Le Beyec, Z. Phys. A **287**, 71 (1978).
16. U. J. Schrewe, W.-D. Schmidt-Ott, R.-D. v. Dincklage, E. Georg, P. Lemmertz, H. Jungclas and D. Hirdes, Z. Phys. A **288**, 189 (1978)
17. A. Bouldjedri, R. Duffait, R. Béraud, A. Emsallem, N. Redon, A. Gizon, J. Genevey, D. Barnéoud and J. Blachot, Z. Phys. A **342**, 267 (1992).
18. W.-D. Schmidt-Ott, H. Salewski, F. Meissner, U. Bosch-Wicke, P. Koschel, V. Kunze and R. Michaelsen, Nucl. Phys. **A545**, 646 (1992).
19. C. N. Davids, *et al*., Phys. Rev. C **55,** 2255 (1997).
20. A. H. Wapstra and K. Bos, At. Data Nucl. Data Tables **17**, 474 (1976).
21. P. Möller, J. R. Nix, W. D. Myers and W. J. Swiatecki, At. Data Nucl. Data Tables **59**, 185 (1995).

FIGURES AND FIGURE CAPTIONS

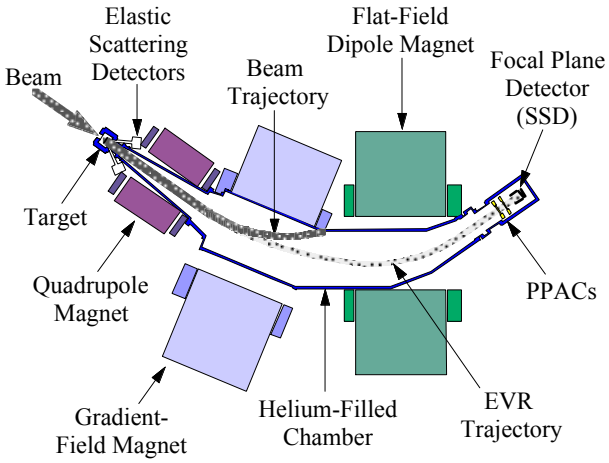

FIG 1. A schematic diagram showing the major components of the Berkeley Gas-Filled Separator.

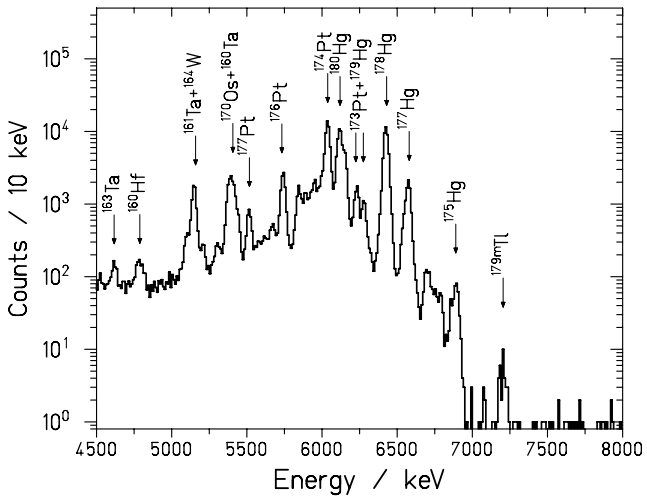

FIG 2. Alpha decay spectrum observed during the beam-off period from a 340 MeV ^{78}Kr bombardment of a 1.05 mg/cm^2 ^{102}Pd target.

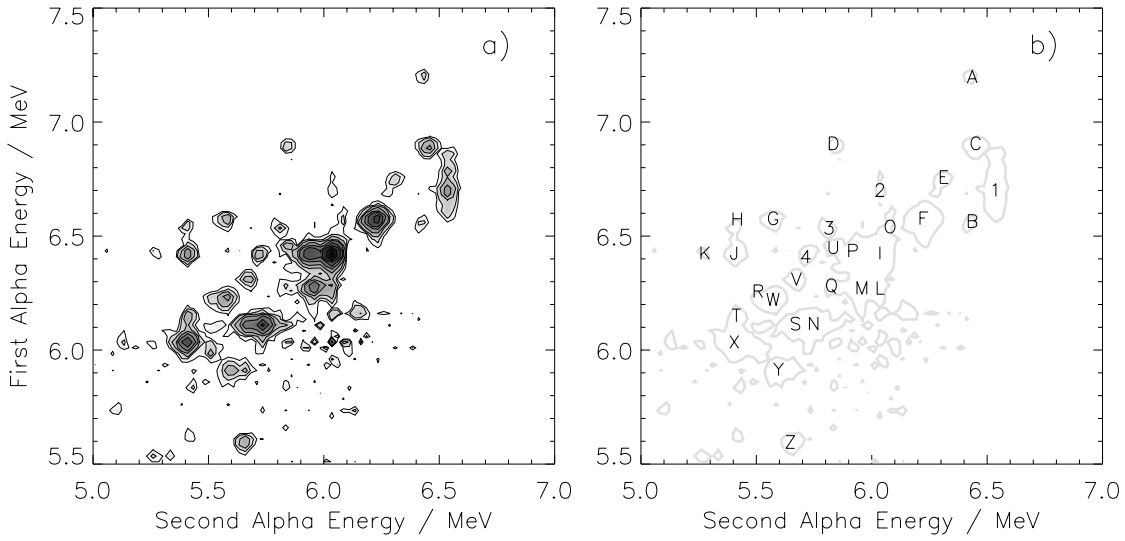

FIG 3. Position-correlated alpha decay pairs observed in the bombardment. The energy of the first alpha decay observed, from the parent, is plotted versus the energy of the second alpha decay, which is usually the daughter but sometimes the grand-daughter. In part a, the number of correlations as a function of parent and daughter energies is shown, with the intensity plotted logarithmically. A Monte Carlo simulation was used to estimate the intensity distribution of random correlations as a function of parent and daughter energies; this has been subtracted from the figure (see text.) In part b, labels associate each peak shown in part a with the pairs of decays listed in Table 1.

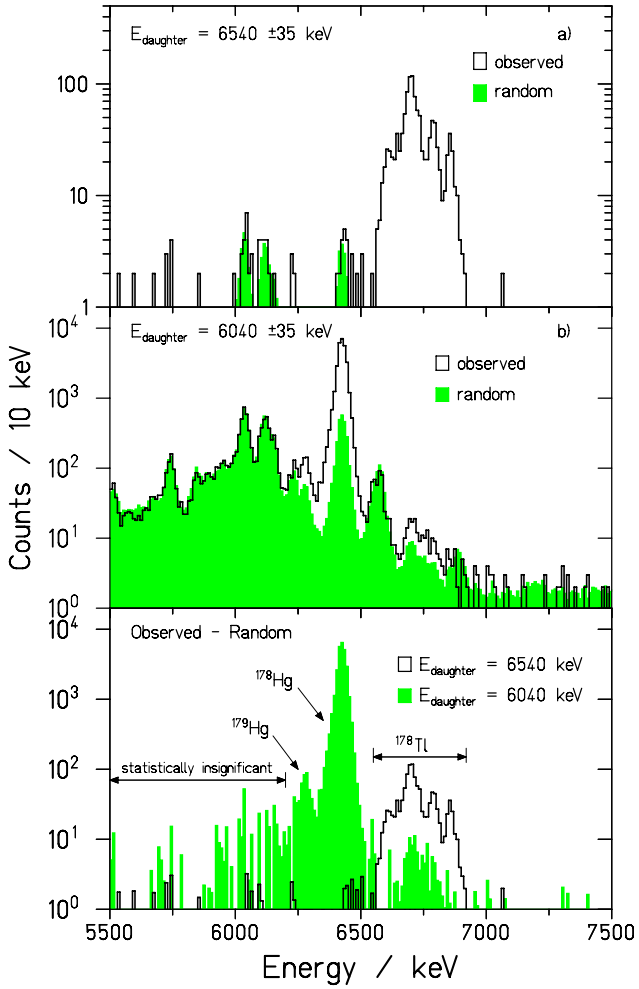

FIG 4. Alpha decays preceding correlated 6.540 ±0.035 MeV and 6.040 ±0.035 MeV alpha decays. The observed correlated events (open), and simulated randomly-correlated events (shaded) are shown for decays preceding 6.540 MeV and 6.040 MeV alpha particles in parts a and b, respectively. These are the primary alpha decay energies for ^{174}Au and ^{174}Pt. In part c, the random correlations have been subtracted from the observed correlations leaving the spectra of alpha emitters with daughters that emit 6.540 MeV (open) and 6.040 MeV (shaded) alpha particles.

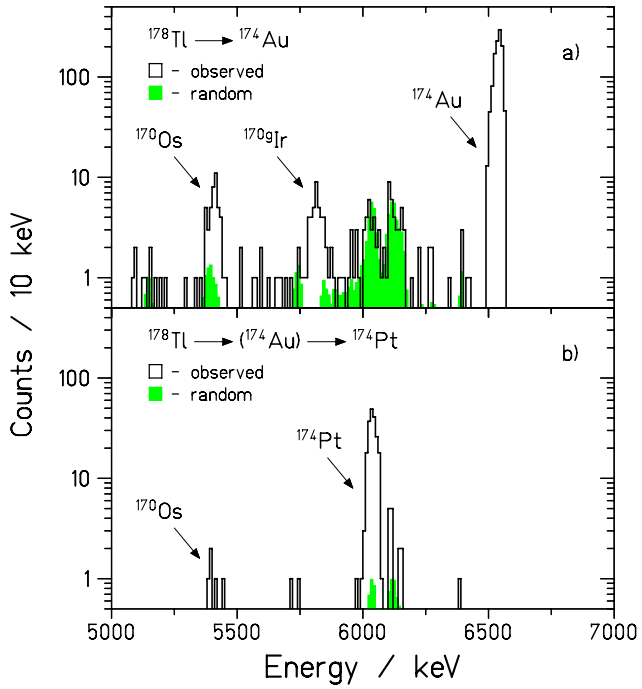

FIG 5. Position-correlated events observed after ^{178}Tl-^{174}Au (a) and ^{178}Tl-^{174}Pt (b) decay pairs. Simulated random correlations are indicated by the shaded histograms.

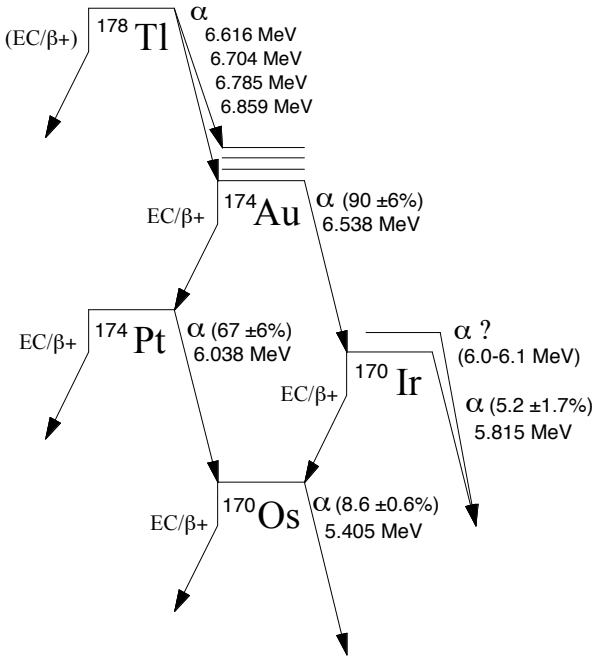

FIG 6. Proposed decay scheme for ^{178}Tl and its daughters, as deduced from the data.

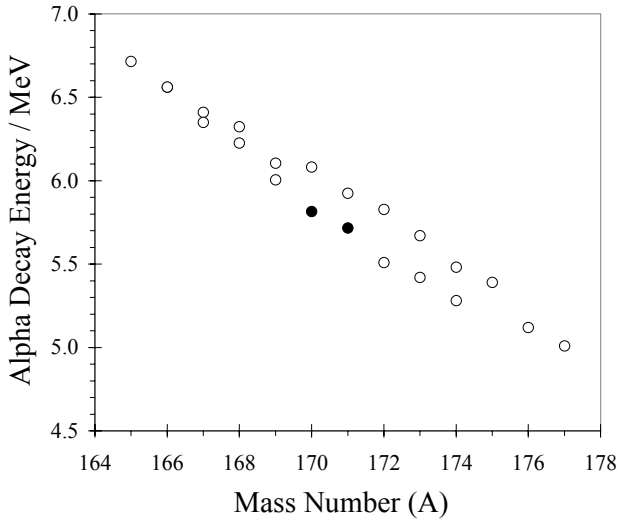

FIG 7. Isomerism in the light Ir isotopes. Observed alpha-decay energies from the literature (open circles) are plotted versus mass number. The filled circles at A = 170 and 171 indicate new transistions deduced from the present work. See text.

TABLES

TABLE I. Correlated alpha-decay pairs observed, as shown in Fig. 3. Unless otherwise indicated, the second decay corresponds to the decay of the daughter nucleus resulting from the first decay. Lettered peaks are assigned based on literature energy values [5-7]. Numbered peaks are assigned based on the present work (see text.)

Peak	First Decay	Energy (MeV)	Second Decay	Energy (MeV)	Peak	First Decay	Energy (MeV)	Second Decay	Energy (MeV)
A	$^{179}Tl^{m}$	7.201	^{175}Au	6.438	P	^{175}Au	6.438	^{171}Ir	5.920
B	^{179}Tl	6.568	^{175}Au	6.438	Q	^{176}Au	6.286	^{172}Ir	5.828
C	^{175}Hg	6.909	^{171}Pt	6.453	R	^{176}Au	6.260	^{172}Ir	5.510
D†	^{175}Hg	6.909	^{167}Os	5.836	S	^{177}Au	6.118	^{173}Ir	5.672
E	^{176}Hg	6.761	^{172}Pt	6.314	T	^{177}Au	6.154	^{173}Ir	5.416
F	^{177}Hg	6.577	^{173}Pt	6.225	U	^{171}Pt	6.453	^{167}Os	5.836
G†	^{177}Hg	6.577	^{169}Os	5.575	V	^{172}Pt	6.314	^{168}Os	5.676
H*	^{177}Hg	6.577	^{173}Ir	5.420	W	^{173}Pt	6.225	^{169}Os	5.575
I	^{178}Hg	6.428	^{174}Pt	6.038	X	^{174}Pt	6.038	^{170}Os	5.407
J†	^{178}Hg	6.428	^{170}Os	5.407	Y	^{163}Re	5.918	^{159}Ta	5.599
K*	^{178}Hg	6.428	^{174}Ir	5.280	Z	^{159}Ta	5.599	^{155}Lu	5.650
L	^{179}Hg	6.275	^{175}Pt	6.038	1	^{178}Tl	6.704	^{174}Au	6.538
M	^{179}Hg	6.275	^{175}Pt	5.960	2*	^{178}Tl	6.704	^{174}Pt	6.038
N	^{180}Hg	6.119	^{176}Pt	5.751	3	^{174}Au	6.538	^{170}Ir	5.817
O	^{174}Au	6.544	^{170}Ir	6.082	4	^{175}Au	6.412	^{171}Ir	5.717

*Parent decay correlated to beta-grand-daughter decay, e.g., $^{178}Tl -\alpha_1-> {}^{174}Au (-\beta->) {}^{174}Pt -\alpha_2-> {}^{169}Os$.

†Parent decay correlated to grand-daughter decay, e.g., $^{175}Hg -\alpha_1-> {}^{171}Pt (-\alpha->) {}^{167}Os -\alpha_2-> {}^{163}W$.

TABLE II. Comparison between half-lives measured in the present work, corrected for random correlation rates as per Equation 1, and literature values taken from Ref. 5 and the references cited therein, unless otherwise noted.

Isotope	Energy (MeV)	Half-Life (ms)		
		Present Work	Page, *et al*.	Other Literature
$^{179}Tl^{m}$	7.201	1.7 ±0.2	$0.7\ ^{+0.6}_{-0.4}$	1.4 ±0.5
^{175}Hg	6.909	10.8 ±0.4	8 ±8	$20\ ^{+40}_{-13}$
^{176}Hg	6.761	20 ±2	18 ±10	$34\ ^{+18}_{-9}$
^{171}Pt	6.453	51 ±2	43 ±3	31 ±5
^{172}Pt	6.314	104 ±7	96 ±3	106 ±7
^{177}Hg	6.577	127 ±2	114 ±15	134 ±5
^{174}Au	6.538	139 ±3	171 ±29	120 ±20
^{175}Au	6.438	158 ±3	185 ±30	200 ±22
^{178}Hg	6.428	269 ±3	287 ±23	255 ±19
^{173}Pt	6.225	370 ±13	376 ±11	342 ±14
^{179}Tl	6.568	415 ±55	430 ±350	160 ±50
^{170}Ir	6.082	430 ±50	830 ±300	–
^{159}Ta	5.599	620 ±50	544 ±16	570 ±180
^{176}Au	6.286	$840\ ^{+170}_{-140}$	–	1250 ±300 [6]
^{179}Hg	6.275	1080 ±90	929 ±114	1090 ±400
^{171}Ir	5.920	$1150\ ^{+130}_{-110}$	1300 ±200	1470 ±80

TABLE III. Summary of observed ^{178}Tl alpha-decay transitions. The half-life determined from all four transitions combined is $254 \pm ^{+11}_{-9}$ ms.

Energy (MeV)	Lit. Energy [3] (MeV)	Q-value (MeV)	relative intensity	half-life (ms)
6.616(15)	–	6.768(15)	0.23	$224\ ^{+25}_{-19}$
6.704(5)	6.71	6.858(5)	1.	$247\ ^{+14}_{-11}$
6.785(5)	6.79	6.940(5)	0.30	$273\ ^{+26}_{-20}$
6.859(5)	6.87	7.017(5)	0.17	$246\ ^{+29}_{-21}$

TABLE IV. Comparison between the predications of various theoretical mass models [11-13,20,21] and the experimental masses derived from the present work, as calculated from the measured decay energies and daughter masses tabulated in Ref. 13.

	mass excess Δ (MeV)		
mass model	^{178}Tl	^{170}Ir	^{171}Ir
Liran-Zeldes (1976)	-3.67	-22.57	-25.58
Möller-Nix (1988)	-3.83	-22.47	-25.69
Möller, *et al*. (1988)	-5.13	-23.26	-26.40
Comay-Kelson-Zidon (1988)	-4.31(91)	-23.58(63)	-26.70(65)
Tachibana, *et al*. (1988)	-5.57	-23.77	-26.72
Janecke-Masson (1988)	-4.84	-23.63	-26.56
Masson-Janecke (1988)	-4.47	-23.97	-26.65
Möller, *et al*. (1995)	-4.87	-23.76	-26.70
Aboussir, *et al*. (1995)	-4.60	-22.80	-26.50
Wapstra-Audi (1995)	-4.45(21)	-23.26(15)	-26.29(13)
daughter mass excess [13]	-14.05(15)	-31.86(14)	-34.87(13)
experiment, this work	-4.61(15)	-23.48(15)	-26.59(14)